PCCP

Accepted Manuscript

ROYAL SOCIETY OF CHEMISTRY

www.rsc.org/pccp

Morphology Effect of Supported Subnanometer Pt Clusters on First and Key Step of CO_2 Photoreduction

Chi-Ta Yang,[1] Brandon C. Wood,[2] Venkat R. Bhethanabotla,[3] Babu Joseph[4]*

[1,3,4]Department of Chemical and Biomedical Engineering, University of South Florida, Tampa, FL, 33620, USA, [2]Quantum Simulations Group, Lawrence Livermore National Laboratory, Livermore, CA 94550, USA.

[1]chita@mail.usf.edu, [2]brandonwood@llnl.gov, [3]bhethana@usf.edu, [4*]bjoseph@usf.edu,

Corresponding Author: *Email: bjoseph@usf.edu. Phone: 813-974-0692.

Keywords: Morphology/Geometry/Size Effect, Structural Fluxionality, CO_2 Reduction, CO_2 Adsorption, Photocatalysis, TiO_2, Subnanometer Pt clusters

Abstract

Using Density Functional Theory calculations, we investigate the influence of size-dependent cluster morphology on the synergistic catalytic properties of anatase TiO_2 (101) surfaces decorated with subnanometer Pt clusters. Focusing on the formation of the key precursor in the CO_2 photoreduction reaction (bent CO_2^-), we find that flatter (2D-like) Pt clusters that "wet" the TiO_2 surface offer significantly less benefit than 3D-like Pt clusters. We attribute the differences to three factors. First, the 3D clusters provide a greater number of accessible Pt-TiO_2 interfacial sites with geometries that can aid the CO_2 bond bending and charge transfer processes. Second, binding competition among each Pt-CO_2 bonding interaction mitigates maximum orbital overlaps, leading to insufficient CO_2 binding. Third and also most interestingly, the 3D clusters tend to possess higher structural fluxionality than the flatter clusters, which is shown to correlate positively with CO_2 binding strength. The preferred morphology adopted by the clusters depends on several factors, including cluster size and the presence of oxygen vacancies on the TiO_2 surface; this suggests a strategy for optimizing the synergistic effect between Pt clusters and TiO_2 surfaces for CO_2 photocatalysis. Clusters of ~ 6-8 atoms should provide the largest benefit, since they retain the desired 3D morphology, yet are small enough to exhibit high structural fluxionality. Electronic structure analysis provides additional insight into the electronic motivations for the enhanced binding of CO_2 on TiO_2-supported 3D Pt clusters, as well as suppressed binding on flattened, 2D-like clusters.

1. Introduction

Oxide-supported subnanometer metal clusters have drawn considerable interest due to their enhanced catalytic activities,[1-6] which is attributed to unique properties of such tiny clusters: dynamic structural fluxionality,[1] larger fraction of under-coordinated surface atoms,[3, 4] and the interactions between the deposited cluster and the support.[7] The application of subnanometer metal clusters is likely to advance the development of promising catalysts and photocatalysts,[8] and the fundamental understanding of the cluster-support interaction has become crucial to such development.[9-12]

Ever since Fujishima and Honda first demonstrated photocatalytic water splitting with TiO_2 electrodes in 1972,[13] numerous researchers have extended the idea to environmental[14] and clean energy[15, 16] related applications. TiO_2 continues to be the standard metal-oxide material for fundamental studies of photocatalysis,[17] although other promising materials with potentially higher photo-efficiencies have been widely explored.[18-20] Techniques for improving the activity of TiO_2 have included the deposition of noble metal nanoparticles[21] as cocatalysts to reduce the recombination of e-/h+ pairs as well as plasmonic particles to increase the concentration of photoexcited electrons.[22, 23] Doping with elements such as N and Ag[24] and creating surface defects[25] have also been used to improve photo-efficiency by modifying the bandgap.

Specifically for CO_2 photoreduction on TiO_2, understanding the reduction mechanism has been a focus of several recent computational studies.[26-30] Among the reduction steps, the highest reduction potential of the first step, CO_2 to CO_2^-, makes it a key step,[31] and one vital factor for the success of this step is the geometry of the adsorbed CO_2 species[27]—specifically, bent-form CO_2. It is easier to transfer photoexcited electrons to bent-form CO_2 thanks to the decrease of the CO_2 LUMO energy as the O-C-O bond angle decreases.[27, 28] Prior first-principles calculations

have investigated this first and key step on different surfaces of TiO_2 using cluster models.[26, 32-34] More thorough studies have considered periodic TiO_2 models with/without oxygen vacancies[28, 35] and interstitial Ti atoms at (sub)surfaces[36]; other oxide surfaces such as Zn_2GeO_4[37] and ceria(110)[38, 39] have also been studied.

Recently, we examined the incorporation of subnanometer Ag and Pt clusters on TiO_2 surfaces, with a specific view towards their role in the mechanisms and energetics of CO_2 photoreduction.[9, 30] First, we explored the structural and electronic properties of the surface-supported clusters, focusing on the binding mechanism, issues related to catalysis (decoration and cluster sintering), and optical absorption behavior.[9] We next examined the synergistic effect between Ag/Pt octamer clusters and the TiO_2 surface in promoting the first and key step of CO_2 photoreduction, finding that Pt clusters in particular can provide new adsorption sites for bent-form CO_2^- anion species.[30]

In this article, we extend our previous results to systematically explore the influence of size-dependent Pt cluster morphology on CO_2 adsorption behavior to shed light on the design of promising photocatalysts for CO_2 photoreduction. Our efforts are motivated in large part by experimental reports demonstrating the role of the cluster size in determining the catalytic behavior in metal/oxide catalysts;[40, 41] other studies[42-46] have further hinted at a more complex relationship connected to the cluster geometry. For instance, Watanabe et al.[42] showed that as the size of Pt_n/rutile TiO_2 varied with n=4, 7-10 and 15, there was a geometrical transition between planar and three-dimensional morphologies at n=8 that corresponded to a significant decrease in activation energy for CO oxidation. Similarly, Kaden et al. reported that for Pd_n deposited on rutile TiO_2 (n=1, 2, 4, 7, 10, 16, 20, and 25), certain intermediate cluster sizes had unusually low catalytic activity, and that the continual increase in the cluster size caused an abrupt increase in

the number of adsorbed cluster layers.[45] These studies point to the possible importance not only of cluster size but also of morphology/geometry as determining factors in catalytic activity.

We use density functional theory (DFT) to analyze the relationship between the cluster size (tetramer, hexamer, and octamer) and the preferred morphology (planar two-dimensional (2D) vs. three-dimensional (3D)), and more importantly to explore how the cluster morphology affects the key precursor formation for CO_2 photoreduction. The choice of the surface was inspired by the fact that anatase TiO_2 (101) is the most stable surface and is the main constituent in the widely used commercial Degussa P25 photocatalyst.[47] The pristine anatase surface (i.e., defect-free surface) is considered as well as the surface with an oxygen vacancy (i.e., reduced surface), since point defects in TiO_2 have been connected to interesting catalytic effects.[10] In addition to analyzing the electronic and structural properties of the bound CO_2 on each of the supported cluster surfaces, we introduce the adsorption-induced displacement (per Pt atom) as a metric of the cluster's structural fluxionality upon CO_2 adsorption. As we will show, this quantity becomes an important additional descriptor of CO_2 binding. Finally, an analysis of C-O bond-breaking tendency and vibrational frequencies associated with adsorption geometries is provided to facilitate comparisons with experiments and to help the development of promising subnanometer metal cluster/semiconductor catalysts for CO_2 photoreduction.

2. Computational Methods

Anatase TiO_2 (101) surfaces are comprised of 2-fold(2c)/3-fold(3c) coordinated O atoms and 5-fold(5c-)/6-fold(6c-) coordinated Ti atoms. The 3c-O atoms can lie between 5-c Ti or 6-c Ti atoms. Following our previous work[30] and others,[28, 36] we model the reduced surface by removing an oxygen atom from a bridge site (2c-O). Stable geometries of the supported Pt clusters were obtained using the method described in our previous work.[9]

The DFT calculations were performed using the VASP (Vienna Ab Initio Simulation package) code.[48-50] Exchange-correlation was represented by the Perdew–Burke–Ernzerhof (PBE) functional of the generalized gradient approximation (GGA),[51] and the electron-ion interactions were modeled by the projector-augmented wave (PAW)[52] method. A kinetic energy cutoff of 500 eV was used for the wavefunctions, and energies were converged to 10^{-5} eV. Spin-polarized calculations were incorporated in all calculations with the force convergence criteria on each atom set to < 0.01 eV/ Å. Because standard DFT improperly describes the strongly correlated d-states in transition-metal oxides, there could be some effect on the charge transfer among the support, clusters, and CO_2 due to electron localization at surface Ti atoms, particularly for the reduced surface. To investigate this possibility, we previously performed a test[30] of CO_2 adsorption on reduced anatase TiO_2 (101)-supported Pt octamers using the DFT+*U* method.[53] Different *U* values (*U*=3.5, 4.0, and 4.5) were found to have very little effect (<1% difference) on the Bader charges of the CO_2 adsorption sites with respect to conventional DFT (this analysis is revisited in terms of the effect of *U* on the character of the electronic states in Fig. S1 of the Supplementary Information). Previous studies concerning the interactions of transition metal clusters[54, 55]/adsorbates[56] with perfect or reduced TiO_2 surfaces also showed similar charge distributions and cluster stability with and without the +*U* correction. Because we are primarily interested in qualitative trends, and in order to maintain compatibility with our previous analyses, [9, 30] the calculations presented here are performed within conventional PBE.

We consider a 3x1 supercell of the anatase TiO_2 (101) surface with six trilayers, in which the bottom three layers were frozen, and the top three layers and metal clusters were relaxed; the vacuum region between the slabs was set to 12 Å. A Monkhorst-Pack [57] mesh of 2x2x1 k-points was used to sample the Brillouin zone for determining the CO_2 adsorption geometries and

energetics; the k-point mesh was increased to 6x6x1 for the density of states (DOS) calculations. The electronic analysis includes atom-projected densities of states (p-DOS) within the energy ranges of interest, and the zero energy position represents the Fermi level in the p-DOS figures. Density plots (DPs) with equal-density isosurfaces of 0.001e/ $Å^3$ are also studied to investigate the binding mechanism. Bader charges[58] are analyzed to understand the charge distribution of CO_2 adsorption sites. The vibrational frequencies are obtained from the frozen-phonon approach with a displacement of 0.015 Å for each atom in the CO_2 molecule. The adsorption energies of CO_2 on the model surface were calculated as the difference between the total energy of the composite system (CO_2 adsorbed on TiO_2-supported Pt clusters) and the sum of total energies of the isolated CO_2 molecule and TiO_2-supported Pt surfaces. We point out that based on a prior comparison of CO_2 adsorption on anatase TiO_2(101) using PBE and PBE + dispersion interactions,[36] the incorporation of dispersion interactions may increase the adsorption energy as well as adsorption sites on supported Pt clusters' surfaces. Nevertheless, our discussion is focused on general trends, which are expected to be insensitive to such details. A more negative adsorption energy indicates more favorable adsorption. The adsorption sites are identified by a notation in which the first letter refers to elemental composition of the cluster ("P" for Pt), the second letter refers to the cluster size ("T/H/O" for tetramer/hexamer/octamer), and a number designates the specific site index. For the reduced surfaces, the site indices are prepended with "Vo" to indicate the presence of an oxygen vacancy.

3. Results

Before analyzing the relationships between cluster size, morphology, and fluxionality with respect to catalysis, it is necessary to begin with an overview of CO_2 binding on the respective surfaces. Results for CO_2 binding on the anatase TiO_2 (101)-supported Pt octamer have already

been reported.[30] Here, we follow an identical recipe for the tetramer and hexamer, focusing on the possible formation of the bent CO_2^- precursor, which facilitates CO_2 activation[28] and leads to the formation of light hydrocarbons. Specifically, we assess four basic ingredients:[30] (i) availability of binding sites, (ii) intermediate adsorption energy at those sites (too strong = traps; too weak = inactive), (iii) adsorption-induced geometry of bent CO_2, and (iv) adsorption-induced charge transfer to the C atom of CO_2. The latter two factors are instrumental in the formation of bent CO_2^-.

In the subsequent sections, results from all three cluster sizes (tetramer, hexamer, and octamer) will be used to analyze the cluster morphology/size-dependent catalytic property. The focus here will be on adsorption sites in direct contact with Pt clusters (Pt related sites): at the interface edge of the Pt clusters and TiO_2 surface ("interface edge site": one O of CO_2 is interacting with the surface 5c-Ti atom while C or the other O with Pt clusters); or else only on the Pt clusters ("Pt only site": 1-Pt only or 2-Pt only sites in which CO_2 interacts with only one Pt or with two Pt atoms of the clusters, respectively).[30] A brief discussion of bridged carbonate configurations not associated with clusters (PT2, PTVo2, PH5, and PHVo7 accordingly in Figure 1b, Figure 3b, Figure 2e, and Figure 4g) is presented in Supporting Information.

The optimized configurations and structural parameters of CO_2 on perfect surface-supported Pt tetramer and hexamer are given in Figure 1 and 2, while those on reduced surface are in Figure 3 and 4, respectively. The corresponding adsorption energy, O-C-O angle of CO_2, and Bader charge difference of the adsorbed CO_2 molecule for each configuration on the clusters decorated perfect and reduced surfaces are reported in Table 1 and Table 2, respectively. Note that upon comparing linear CO_2 adsorption on a reduced TiO_2 surface in our previous study[30] to similar models incorporating NEB and MD simulations,[59] we speculate that CO_2 adsorption sites

with energies around or below 0.36eV could become unstable at room temperature once thermal fluctuations are considered.

3.1 CO_2 Adsorption on Perfect TiO_2-Supported Pt Clusters

Previously, we found that the Pt octamer/perfect TiO_2 surface offers adsorption sites for bent form CO_2, and that these CO_2 bind rather strongly compared to those on the pure TiO_2 surface.[30, 36] We find that the Pt hexamer/perfect surface follows the same trend, and is even better in these two aspects; however, the supported Pt tetramer does not exhibit any such advantages. Note that the deposited tetramer and hexamer retain a 3D geometry, as we previously found for the deposited octamer on the same surface.[9, 30] On the supported Pt tetramer surface, our technique identified three CO_2 adsorption sites (PT1-PT3 in Figure 1a-c); however, two of these (PT2 and PT3) are metastable (i.e., positive adsorption energies that may be kinetically stabilized) and feature adsorbed CO_2 not in direct contact with Pt. In contrast, seven sites (PH1-PH7 in Figure 2a-g) were found for hexamer case, only one of which (PH7) is metastable. Six of these sites (all except PH5) feature direct contact with Pt. We point out that three such sites were previously found for the octamer (all stable).[30]

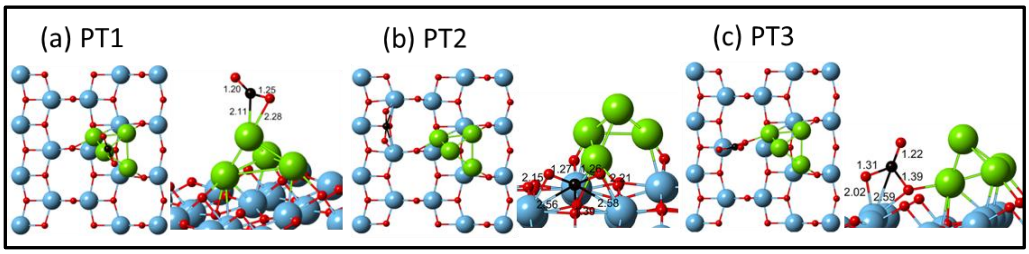

Figure 1. Stable CO_2 adsorption configurations on the perfect anatase TiO_2(101) surface in the presence of Pt tetramers (O in red, C in black, Ti in blue, and Pt in green. The numbers indicate the bond lengths in Å).

For the perfect surface-supported tetramer, PT1 is a 1-Pt only site and the only stable configuration obtained. No interface edge sites are observed. The O-C-O angle for this adsorbate

differs from that observed in the Pt hexamer & octamer cases, and may be a characteristic specific to CO_2 adsorbed on the supported Pt tetramer. The Bader charges indicate the formation of a CO_2^- anion in the PT1 configuration. Interestingly, the metastable PT3 reveals the formation of a carbonate-like molecule upon CO_2 adsorption, facilitated by reconstruction of the TiO_2 surface in which the distance of the bridge oxygen and the 6c-Ti atom is increased by ~0.6 Å.

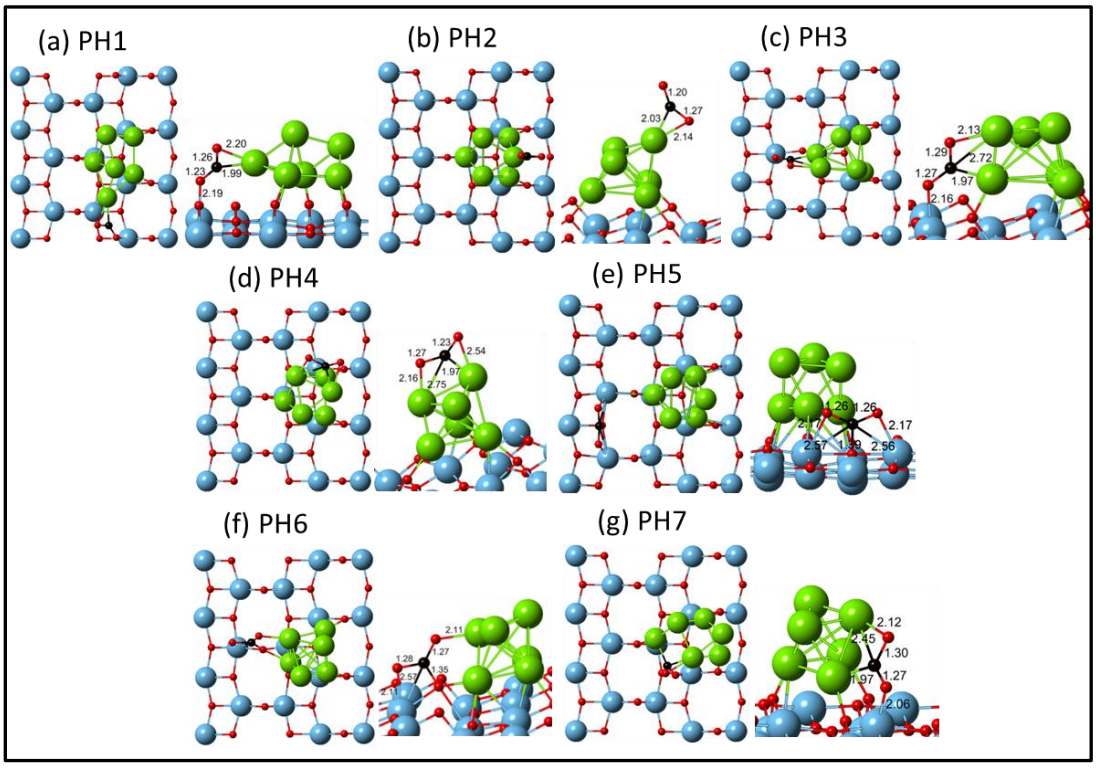

Figure 2. Stable CO_2 adsorption configurations on the perfect anatase TiO_2(101) surface in the presence of Pt hexamers (O in red, C in black, Ti in blue, and Pt in green. The numbers indicate the bond lengths in Å).

For the perfect surface-supported hexamer, PH1, PH3, and PH7 (Figure 2a, c, and g) are interface edge sites. Notably, PH1 is the most stable site among all Pt tetramer, hexamer, and octamer configurations we found. In this configuration, structural distortion of the hexamer (reflected by comparing deposited hexamers in Figure 2a & e) causes one Pt atom to primarily interact with CO_2. Although this type of CO_2-Pt interaction was not previously found on the

perfect surface-supported Pt octamer, we did observe it on the reduced surface-supported Pt octamer; the difference may result from the ease of the Pt octamer to modify its geometry due to the presence of the oxygen vacancy. PH3 is an analogous structure that was previously observed in the perfect surface-supported octamer,[30] and the structural and electronic properties are quite similar in both cases. The metastable PH7 site is similar to PH3, but binds more weakly. PH6 is weakly stable, and is similar to PT3 in featuring a carbonate-like molecule. PH2 and PH4 are stable 1-Pt only and 2-Pt only sites. Corresponding configurations were previously found on the perfect surface-supported octamer[30] with similar structural parameters except for a longer binding distance between O in CO_2 and the Pt atom in the configuration analogous to PH2. However, PH2 also has a much higher binding strength by 0.56eV and more negative charge accumulation in C compared to the analogous octamer configuration.

Table 1. Calculated properties[a] based on CO_2 adsorption configurations on perfect anatase TiO_2 (101) in the presence of Pt tetramer and hexamer.

Ads. Config.	-Eads(eV)	∠OCO(deg.)	Δe of CO2			ν(CO2)(cm-1)		
			C	O	O	ν1	ν2	ν3
PT1**	0.22	151.2	0.337	-0.078	-0.023	1161	594	1989
PT2	-0.01	133.5	-0.002	0.036	0.061	1259	801	1663
PT3	-0.07	130.0	0.006	0.075	-0.013	1161	788	1695
PH1*	1.01	137.1	0.508	0.061	-0.111	1165	707	1742
PH2**	0.72	146.6	0.432	-0.025	-0.109	1114	650	1927
PH3*	0.71	125.9	0.602	0.037	-0.064	1180	764	1483
PH4**	0.64	136.6	0.497	-0.039	-0.051	1163	734	1694
PH5	0.08	133.3	-0.012	0.055	0.047	1263	804	1654
PH6	0.01	125.9	-0.023	0.020	-0.001	1262	833	1541
PH7*	-0.04	123.5	0.632	0.058	-0.063	1163	738	1434

[a]Values represent the adsorption energy, O-C-O angle of CO_2, difference of Bader charge of CO_2 molecule upon adsorption, and vibrational frequencies of symmetric (ν1), bending (ν2), and asymmetric (ν3) stretching modes (Δe >0 means electron accumulation; PT and PH represent Pt tetramer and Pt hexamer, respectively; single and double asterisks indicate interface edge and Pt only sites, respectively).

In summary, Pt tetramers on perfect anatase provide significantly fewer binding sites for CO_2 compared with octamers[30] or hexamers, while hexamers provide the most. This likely reflects the smaller contact area of the Pt tetramer. The Pt tetramer also exhibits the weakest binding with CO_2. On the perfect surface, Pt hexamers share many common features with octamers in terms of the favored CO_2 binding sites, which leads to similar binding geometries of the adsorbed CO_2. On average, the hexamer exhibits the strongest binding among the three cluster sizes investigated. As we will demonstrate, the general attractiveness of the hexamer over the octamer in terms of binding sites and strength is related to the structural fluxionality of the former.

3.2 CO_2 Adsorption on Reduced TiO_2-Supported Pt Clusters

In contrast with the perfect surface, deposited tetramers and hexamers on reduced surfaces tend to exhibit planar geometries (2D), tending surprisingly to "wet" this surface. This behavior, especially apparent on the hexamer case, was not previously observed on Pt octamers/reduced TiO_2 surfaces,[30] and seems unique to clusters smaller than the hexamer. This also reveals that the cluster morphology/size is an important factor for CO_2 adsorption.

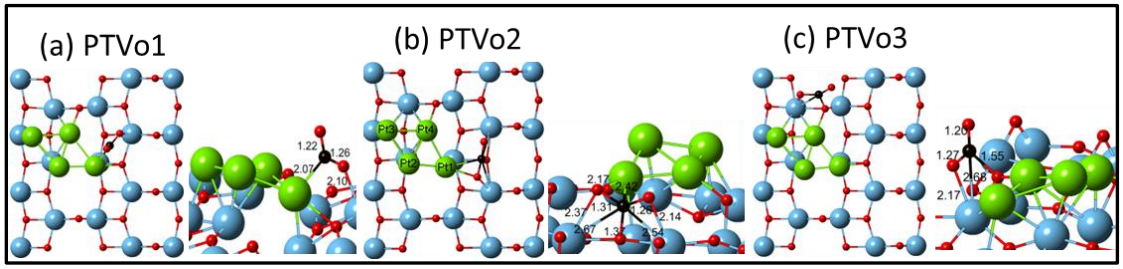

Figure 3. Stable CO_2 adsorption configurations on the reduced anatase TiO_2(101) surface in the presence of Pt tetramers (O in red, C in black, Ti in blue, and Pt in green. The numbers indicate the bond lengths in Å).

Only one stable Pt related site (PTVo1 in Figure 3a) was found on the supported Pt tetramer surface, which closely matches what was found on the tetramer-decorated perfect surface. This

points to that the smaller contact area of the supported Pt tetramers, which limits CO_2 binding. Notably, one difference between the perfect and reduced surfaces for the tetramer is that the Pt-only tetramer site found on the perfect surface is not found on the reduced surface. This may be due to the 2D geometry of the adsorbed Pt tetramer on the reduced surface, which makes insufficient orbital overlaps with CO_2 to form a bonding orbital.[9] Note that PTVo3 (Figure 3c) is a bidentate carbonate species with a tilted adsorbed CO_2.

On the other hand, the hexamer behaves very differently on the perfect and reduced surfaces. In particular, although six Pt related configurations (PHVo1-PHVo6 in Figure 4a-f) were found on the reduced surface-supported Pt hexamer, most of these (PHVo3-PHVo6) are metastable—some with significantly positive adsorption energies—and only two (PHVo1 and PHVo2) are stable. This contrasts sharply with the five stable Pt related sites found for the perfect surface-supported hexamers. Notably, the difference between the two host surfaces in the case of the hexamer cannot be attributed exclusively to the cluster size (contact area limitation), suggesting the importance of other crucial factors. PHVo2, PHVo3, PHVo4, and PHVo6 (Figure 4 b, c, d, and f) are interface edge sites. Of these, only PHVo2 is stable, but the CO_2 binding remains too weak for effective catalysis. All features binding with one Pt atom, which is different from the perfect surface-supported hexamer/octamer where interactions with two Pt atoms exist. This can be understood from the quasi-2D structure of the hexamer as it "wets" the reduced surface, which tends to inhibit simultaneous accessibility to two Pt atom interactions.

Interestingly, the structural parameters and electronic properties of CO_2 for the metastable interface edge sites on the reduced surface-supported hexamer (PHVo3, PHVo4, and PHVo6) are very similar to the stable interface edges in Pt octamer and perfect/hexamer cases, and are attractive for the formation of the bent CO_2^- precursor both in terms of O-C-O angle and charge

transfer to C. The apparent discrepancy between the strongly modified properties of adsorbed CO_2 (which differs between reduced and perfect surfaces) points to a significant role of the cluster geometry cluster (e.g., 2D for the reduced surface-supported hexamer vs. 3D for the perfect surface-supported hexamer) in determining the CO_2 adsorption and catalytic properties.

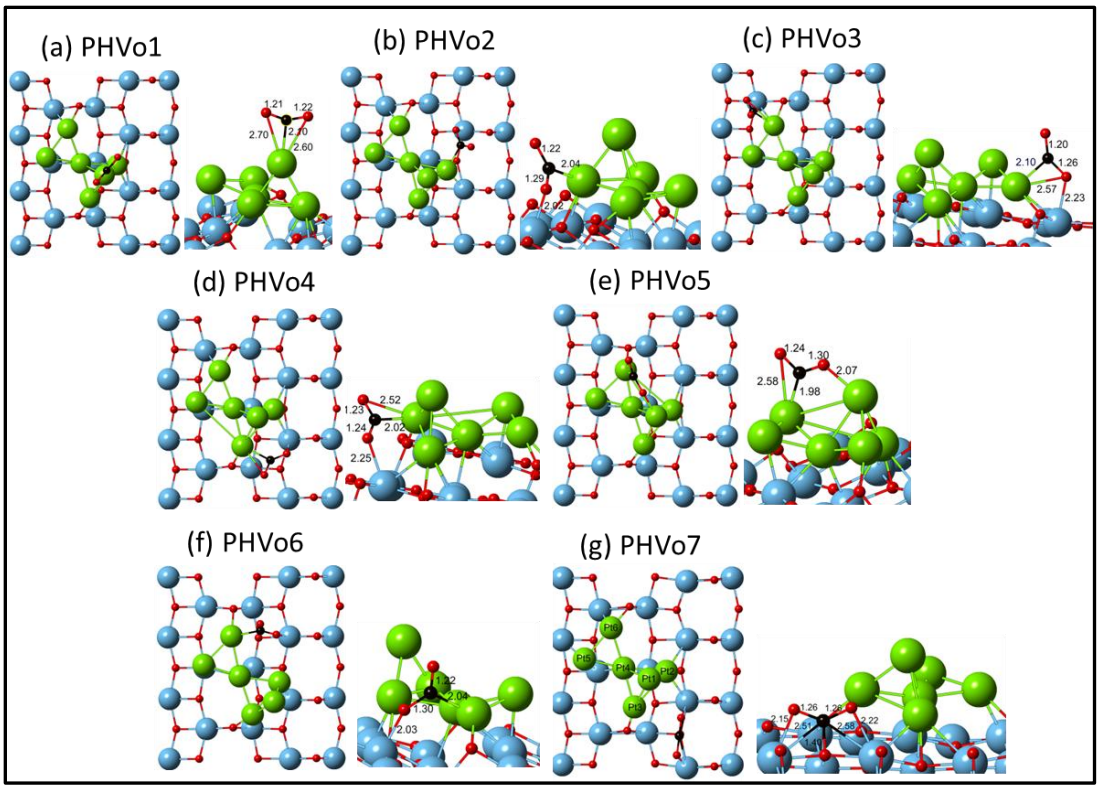

Figure 4. Stable CO_2 adsorption configurations on the reduced anatase TiO_2(101) surface in the presence of Pt hexamers (O in red, C in black, Ti in blue, and Pt in green. The numbers indicate the bond lengths in Å).

The stable PHVo1 and metastable PHVo5 (Figure 4 a & e) represent Pt only sites. Note that the O-C-O angle in PHVo1 is very close to that in the perfect surface-supported tetramer PT1 configuration (154.7° vs. 151.2°), and this angle similarity seems to relate to the geometry of the clusters. Specifically, the geometry of the tetramer on the perfect surface (pyramid-like) can be considered as part of the geometry of the hexamer on the reduced surface. The trend of net charge transfer in CO_2 molecules adsorbed on PT1 and PHVo1 is also quite similar. We point

out that PHVo5 represents the only metastable Pt-only site among all the systems we have studied; this may be related to the unusually small O-C-O angle (126.9°).

Table 2. Calculated properties[a] based on CO_2 adsorption configurations on reduced anatase TiO_2 (101) in the presence of Pt tetramer and hexamer.

Ads. Config.	-Eads(eV)	∠OCO(deg.)	Δe of CO2			ν(CO2)(cm-1)		
			C	O	O	ν1	ν2	ν3
PTVo1*	0.22	136.2	0.437	0.038	-0.028	1182	699	1788
PTVo2	-0.06	131.1	0.114	-0.003	0.033	1191	762	1532
PTVo3	-0.97	137.4	0.117	0.048	0.015	1163	699	1858
PHVo1**	0.16	154.7	0.341	-0.053	-0.047	1181	574	1996
PHVo2*	0.02	131.8	0.530	0.000	0.011	1121	720	1706
PHVo3*	-0.03	140.4	0.392	-0.004	-0.004	1150	648	1858
PHVo4*	-0.13	138.9	0.419	-0.041	0.044	1194	686	1774
PHVo5**	-0.33	126.9	0.596	-0.034	-0.053	1124	740	1593
PHVo6*	-0.41	130.2	0.510	-0.006	0.036	1095	714	1710
PHVo7	-0.83	133.5	-0.017	0.050	0.040	1262	792	1680

[a]Values represent the adsorption energy, O-C-O angle of CO_2, difference of Bader charge of CO_2 molecule upon adsorption, and vibrational frequencies of symmetric (ν1), bending (ν2), and asymmetric (ν3) stretching modes (Δe >0 means electron accumulation; PT and PH represent Pt tetramer and Pt hexamer, respectively; Vo represents an oxygen vacancy; single and double asterisks indicate interface edge and Pt only sites, respectively).

4. Discussion

We begin our discussions by understanding the different geometry reconstructions the same cluster exhibits on the two different host surfaces (perfectly stoichiometric & reduced). The morphology-dependent factors on CO_2 adsorption are then investigated with additional electronic insights into the bound CO_2, following which experimental observables are connected to electronic & geometry information, adsorption sites, and C-O bonding breaking tendency of the bound CO_2.

4.1 Geometry Change of Adsorbed Clusters (2D->3D)

Observing the adsorbed tetramer and hexamer on the reduced surface, both clusters tend to evolve toward flat (2D) geometries as compared to the 3D geometries of both clusters on the perfect surface. We find that the driving force for the conversion to quasi-2D geometries is due to the tendency of Pt tetramer and hexamer to form bonding orbitals with surface Ti atoms (especially 4c-Ti and 5c-Ti exposed by the presence of the oxygen vacancy). This is consistent with our previously developed binding mechanism of Pt_n (n=2, 4, and 8) on perfect anatase TiO_2 (101) surface,[9] which suggests that Pt clusters have a strong tendency to bind with surface Ti atoms; the underlying factor is the sufficient orbital overlaps of Pt clusters and surface Ti atoms to form bonding orbitals.

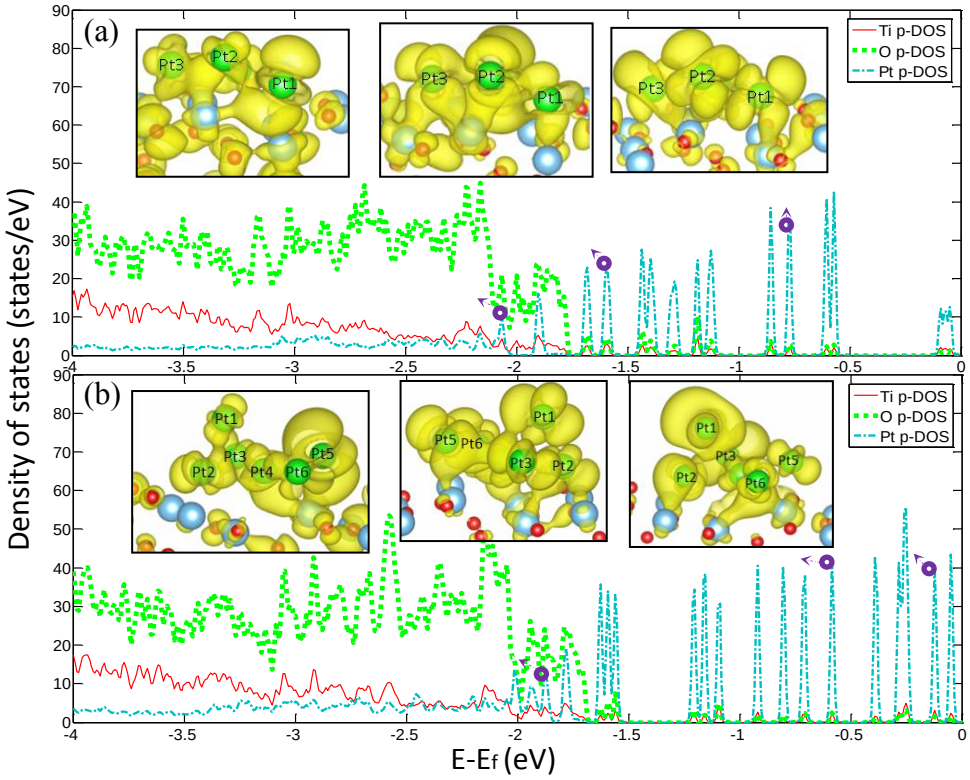

Figure 5. p-DOSs (Ti, O, and Pt) and density plots of reduced anatase TiO_2(101) surface-supported Pt clusters: (a) tetramer and (b) hexamer. The insets show the density plots at corresponding positions: (a) -0.77, -1.60, and -2.05eV and (b) -0.12, -0.58, and -1.77eV (Shown in the figures correspond to spin up).

To see this, we examine the p-DOSs of O, Ti, and Pt atoms of the supported tetramer and hexamer (Figure 5). Resonant peaks can be seen consisting of Ti, O, and Pt atoms, which suggests the disposition of Pt clusters to bind with Ti and O atoms. Further investigations of density plots (DPs) show bonding orbitals formed by the cluster and 4c-Ti; for example, DP at -1.60eV in Figure 5a shows Pt2 & Pt3 of the tetramer binding with 4c-Ti, and DP at -1.77eV in Figure 5b shows Pt5 of the hexamer binding with 4c-Ti. The binding with 5c-Ti can also be seen; for example, DP at -2.05eV in Figure 5a shows Pt1 of the tetramer binding with 5c-Ti, and DP at -0.58eV in Figure 5 b shows Pt2 of the hexamer binding with 5c-Ti. Our result is also consistent with other DFT calculations. Gong et al.[10] obtained the result that Pt_n(n=1-3) prefer to bind with the surface Ti & O atoms of anatase TiO_2(101), and 4c-Ti & 5c-Ti atoms are favored in the presence of oxygen vacancy. A study of Pt_n(n=4-8) supported on rutile TiO_2(110) surface[60] also pointed out the importance of the Pt-Ti bond on the cluster-support binding strength, and showed that two-layer structures are preferred for Pt_5-Pt_8 except Pt_6, which favors planar geometry.

4.2 Geometry-Dependent Binding Mechanism

In our previous investigations of the binding mechanism regarding CO_2 adsorption on perfect/reduced anatase TiO_2 (101)-supported Ag & Pt octamers,[30] we found that for CO_2 adsorption in contact with Pt octamers, binding is facilitated by the hybridization of the molecular orbitals of CO_2 with d orbitals of the Pt atoms. Here, beyond our prior understanding, as Pt clusters can interchange between 3D, 2D planar, and intermediate (3D/2D) geometries depending on the cluster size and substrate, we find that fluxionality plays an additional important role in the CO_2 adsorption. The binding competition between Pt atoms with the adsorbate is also found to be relevant.

First, we revisit the electronic analysis of the Pt binding sites, focusing on comparisons among the three types of Pt-related sites: interface edge, 1-Pt only, and 2-Pt only sites. In our previous study, we showed DOS and DPs of the interface edge and Pt only sites involving two Pt atoms;[30] in this study, we add results for the 1-Pt only site (based on the PH2 site from Figure 2b) in Figure 6. Prior work of the adsorbate-transition metal interactions[61, 62] suggests that the hybridization of adsorbate valance states with the valance states of the metal surface atoms leads to the formation of bonding and antibonding states. For instance, in H-metal (Ni, Cu, Pt, and Au) surface systems, the dominant H 1s-metal d bonding states lie within -10 and -5 eV.[61]

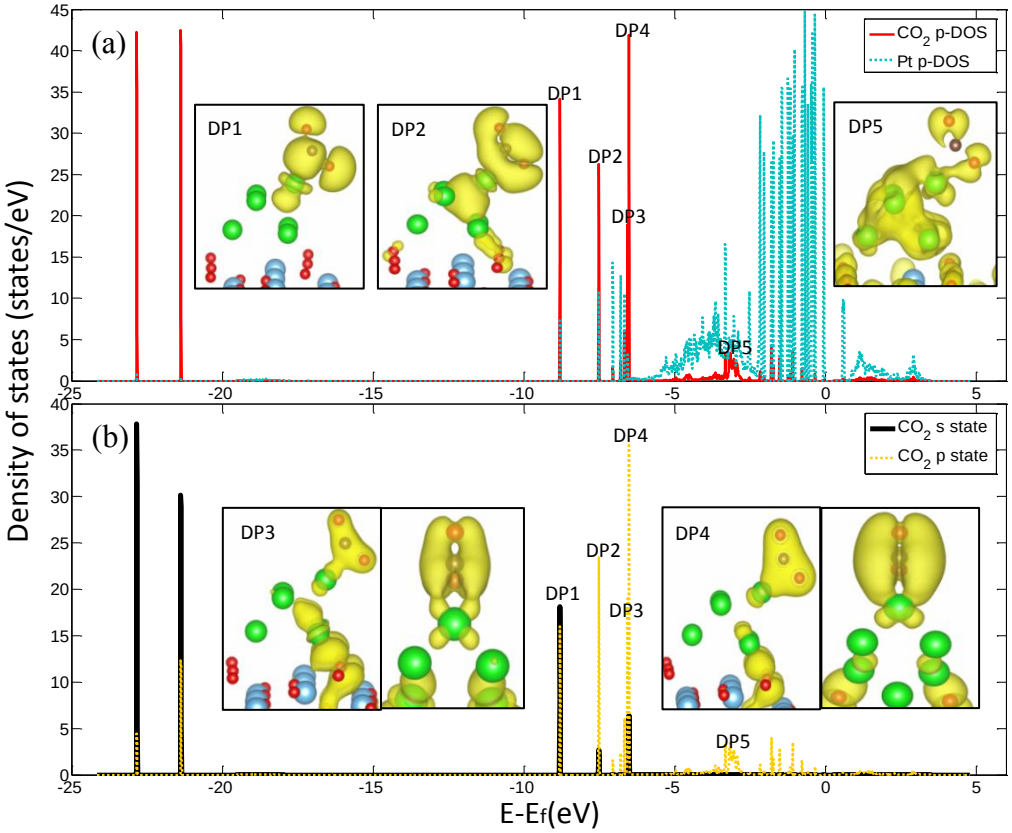

Figure 6. p-DOSs and associated density plots (DPs) of specific states formed upon CO_2 adsorption directly on the Pt hexamer involving one Pt atom (PH2): (a) p-DOSs of the adsorbed CO_2 and Pt; (b) p-DOSs of s and p states of the adsorbed CO_2. DP1-DP5 are the same states in both figures accordingly at -8.80, -7.50, -6.66, -6.55, and -3.30 eV (Shown in the figures correspond to spin up).

In the CO_2-TiO_2 supported Pt hexamer interaction, the resonance peaks of Pt and CO_2 in Figure 6 (a) suggest similar bonding states, again lying mainly between -10 and -5 eV; this is also the same range we found in CO_2-TiO_2 supported Pt octamers.[30] In general, Figure 6b shows that for CO_2, its s states dominate in lower energy levels and p states in higher energy levels. Furthermore, DP1 ($2\sigma_g$), DP2, and DP3 & DP4 ($1\pi_u$) in Figure 6a&b explicitly show CO_2 (s&p)-supported Pt hexamer bonding states consisting of bonding orbitals of CO_2 and d states of the Pt atom. The results are fully consistent with what we previously found for the CO_2-supported Pt octamer interaction of the interface edge and 2-Ptonly sites, leading us to conclude generally that for CO_2-TiO_2 supported Pt subnanometer clusters, CO_2 (s&p) - metal d interactions dominate the bonding states. Note that the DPs in Figure 6 show that in effect only the host Pt atom is involved in the adsorption at the Pt-only site, indicating a local interaction.

Comparing the three types of sites, we also find that the interface edge sites seem to have the strongest CO_2 binding strength (on average), probably due to extra bonding stabilization from CO_2 with surface O atoms. However, there is no consistent pattern in the CO_2 adsorption energies at Pt only sites involving one and two Pt atoms, suggesting that the CO_2 binding strength is not necessarily related to the number of Pt atoms involved.

4.2.1 Structural Fluxionality

Having assessed the electronic origins of the binding mechanism, we next investigate factors for CO_2 adsorption that are connected to cluster morphology. Geometric reconstructions are apparent for supported Pt clusters upon CO_2 adsorption, especially for Pt clusters with 3D geometry. For example, the Pt hexamer in PH1 (Figure 2a) undergoes considerable geometry modification upon CO_2 adsorption (e.g., compare with PH5 in Figure 2e, which is almost the same Pt hexamer geometry as the most favored deposited hexamer when no CO_2 molecule is

present). This geometry reconstruction is associated with a key characteristic of the subnanometer metal cluster, structural fluxionality:[1] during the interaction of CO_2 with the cluster, the cluster tends to vary its geometry to maximize orbital overlaps of the cluster and CO_2, which sustains binding through the formation of the strong bonding orbitals.

To quantify this tendency, we define a quantity called displacement (per Pt atom) to represent the extent of the cluster's structural fluxionality as the equation below (a cluster-center based definition was also tested, shown in Supporting Information):

$$\text{Displacement (structural fluxionality)} = \frac{\sum_n \sqrt{(X_{nf}-X_{ni})^2+(Y_{nf}-Y_{ni})^2+(Z_{nf}-Z_{ni})^2}}{N}$$

, where X, Y, and Z represent the coordinates of the n^{th} atom in the cluster; i and f represent the initial and final states; and n= 1-N, where N equals the cluster size. Considering all CO_2 adsorption configurations obtained in this (supported Pt tetramer and hexamer) and our previous (supported octamer[30]) studies, we evaluate the displacement of 3D, intermediate 3D/2D, and planar 2D Pt clusters (shown in Figure 7a for interface edge sites and in Supporting Information for Pt-only sites). The Pt-only sites show comparable fluxionality capability for all three Pt cluster geometries (3D, 3D/2D, and 2D) upon CO_2 adsorption, which is apparent because the CO_2 adsorbate is unconstrained and can easily modify its own molecular geometry upon adsorption instead of that of the deposited clusters. However, at interface edge sites, 3D, 3D/2D, and 2D show different structural fluxionality capability. 3D geometries [PO1(BP1)[30], POVo1(BPVo1)[30], POVo4(BPVo4)[30], POVo6(BPVo6)[30], PH1, PH3, and PH7] tend to have high displacement values on average, indicating large geometry changes during the CO_2 adsorption. The 3D/2D geometry (PHVo2, PHVo3, PHVo4, and PHVo6) show smaller displacements; but, as seen from the optimized geometries (Figure 4), the displacements mostly come from

horizontal shifts. The 2D geometry exhibits very limited reconstruction. This is because the 2D structure binds tightly with surface atoms, restricting its self-modification, while top layer atoms of the 3D structure are less restricted, giving greater freedom for 3D clusters to reconstruct.

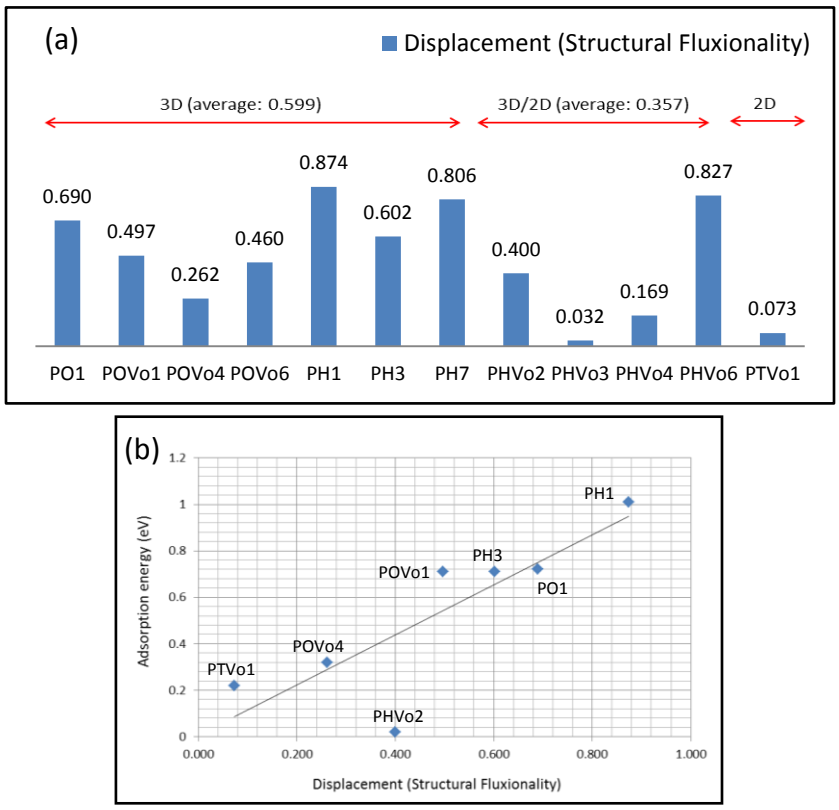

Figure 7. (a) Displacement (Structural fluxionality tendency) of all stable and metastable CO_2 adsorption sites located at the interface edge on the anatase TiO_2(101)-supported tetramer, hexamer, and octamer; (b) Displacement versus adsorption energy of the stable interface edge sites [Octamer data[30]: PO1(BP1), POVo1(BPVo1), POVo4(BPVo4), and POVo6(BPVo6); PO, PH, and PT represent Pt octamer, hexamer, and tetramer; Vo represents an oxygen vacancy].

Displacement (structural fluxionality) is also related to the CO_2 binding strength, which is plotted Figure 7b of stable interface edge sites. As can be seen, there is a positive correlation of displacement and the CO_2 adsorption energy (note: the displacement of PHVo2 mainly comes from horizontal shifts), which means that the more the cluster can modify its geometry, the better orbital overlap is achieved, resulting in stronger CO_2 binding strength. The importance of

structural fluxionality and its connection to particle geometry explains why the Pt hexamer & hexamer on the reduced surface exhibited far fewer stable binding sites than on the perfect surface. On the reduced surface, the vacancy-induced 3D → 2D geometry change leads to lower structural fluxionality, which effectively offsets the benefits associated with interfacial edge sites.

4.2.2 Binding Competition

Though the hybridization of bonding states of CO_2 with d states of the Pt atoms sustains the binding as detailed above, this same interaction can also cause instabilities in the CO_2 adsorption when two Pt atoms act in competition. For instance, considering the major bonding states of the CO_2-Pt clusters/TiO_2 (-10 eV to -5 eV), the DP at -6.00 eV of PHVo5 (Figure 8a) indicates the presence of two competing forces on the CO_2 molecule due to bonding interactions of Pt1 and Pt6 individually, which actually destabilizes binding and leads to a metastable configuration. This is made clearer by comparing the Pt-C-Pt angle to the corresponding stable geometries. The Pt-C-Pt angles in PH4 (Figure 2d) and for two configurations found on supported Pt octamers[30] are 71.3°, and 64.9° & 64.3°, which are all considerably smaller than the 94.8° of the metastable PHVo5. It is understood that when two Pt atoms act in concert, the net force acting on CO_2 with smaller Pt-C-Pt angles can stabilize the adsorbate; on the other hand, with larger angles, the Pt-CO_2 stabilizing forces become smaller, and the forces start to cancel each other due to both Pt atoms competing with each other to bind with the adsorbate. Additional evidence of binding competition destabilizing adsorption strength can be found in PHVo6 (Figure 4f). Looking at the DP at -6.48 eV (Figure 8b), it is seen that in addition to CO_2's binding with Pt6, binding with surface O atoms is also present (which is the reason for the tilted CO_2 geometry); it is suggested that the latter interaction may disturb orbital overlaps of the CO_2 with lobes of the d states of the Pt atom and draw electron density out of the Pt-C bond.

In light of the above analysis, we can further speculate about why 2D planar clusters do not tend to provide additional binding sites on the top surface, as one might expect; this behavior is most obvious for the 2D Pt tetramer (refer to Figure 3). We propose that the reason is due to two factors: limited structural fluxionality and binding competition. A likely scenario is that CO_2 diffuses to the 2D surface, lying horizontally. The binding of C with a Pt atom initiates the adsorption process pulling the CO_2 molecule, followed by a neighboring Pt atom trying to bind with the adsorbate. Then, each Pt atom attempts to maximize overlap with the CO_2 orbitals, but the binding of Pt with surface Ti atoms restricts the geometric modifications necessary for the Pt tetramer to satisfy both overlaps. The Pt-C-Pt angle remains large, and the two pulling forces begin to compete against one another, resulting in weakened CO_2 binding and ultimately desorption.

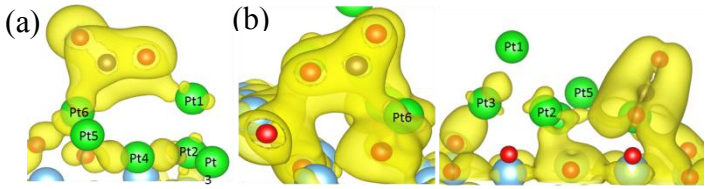

Figure 8. (a) The DP at -6.00 eV of PHVo5; (b) the DP at -6.48 eV of PHVo6.

4.3 CO_2 Bond Breaking tendency

To promote the formation of light hydrocarbons via CO_2 photoreduction, the breaking of the C-O bond of the CO_2 molecule is a crucial factor. Characterization of the CO_2 bond-breaking tendency is possible using current characterization capabilities.[63-66] These studies have shed significant light on the nature of CO_2 photoreduction on subnanometer metal cluster-based photocatalysts. Freund summarized the characterization tools such as LEED and NEXAFS that can be used to gain information of CO_2 geometry.[63] For instance, NEXAFS has been used to show the geometries of CO_2 species on Ni(110).[64] IRRAS along with computational results also

revealed the CO_2 structure on rutile $TiO_2(110)$[65] and $ZnO(10\bar{1}0)$.[66] In our previous study involving CO_2 on supported Pt octamers,[30] we suggested that the charge transfer to C and the O-C-O angle of CO_2 were related to the formation of the bent CO_2^- anion, and by extension to photocatalytic bond activation. Here, we directly show that these two factors correlate with the C-O bond-breaking tendency across all tetramer, hexamer, and octamer configurations, further confirming their importance in CO_2 photoreduction.

The C-O bond breaking is attributed to the electronic population of the antibonding orbitals of the CO_2 molecule. For instance, evidence for antibonding states below the Fermi level for stable hexamer sites is shown in DP5 (Figure 6a), which suggests hybridization of nonbonding CO_2 orbitals (HOMO, $1\pi_g$) with Pt d states. A similar conclusion is also supported by another study regarding the chemistry of the CO_2 molecule, in which bent-form CO_2 resulted in the lowering of the $2\pi_u$ energy, even lower than $1\pi_g$.[63] In Figure 9, we examine the tendency for bond breaking by considering all the CO_2 adsorption sites in contact with the Pt clusters: tetramer (PT1 in Figure 1a, and PTVo1 in Figure 3a), hexamer (PH1-PH4 & PH7 in Figure 2a-d & g, and PHVo1-PHVo6 in Figure 4a-f), and octamer (PO1-PO3 representing BP1-BP3 in Figure 1d-f, and POVo1-POVo4 & POVo6 representing BPVo1-BPVo4 & BPVo6 in Figure 2d-g&i of our previous work[30]). As shown in Figure 9a, a clear correlation between the negative charge accumulation at C of CO_2 and the C-O bond length is found (except POVo6, which represents a metastable configuration). The greater the electron accumulation at C is, the longer the C-O length, which can be attributed to the filling of antibonding states of CO_2. A DFT calculation using the Gaussian09 program package[67] with the B3LYP functional[28] comparing CO_2 and the CO_2^- anion was performed to reveal the role of C in the hybridization of antibonding states. Natural bond orbital (NBO) charge analysis[68] shows the C of CO_2 possessing +1.02*e* with

an average C-O bond length of 1.16Å, while the C of CO_2^- anion possesses +0.50*e* with an average C-O bond length of 1.23Å. This indicates that as C gains electrons, the length of the C-O bond also increases, in agreement with Figure 9a.

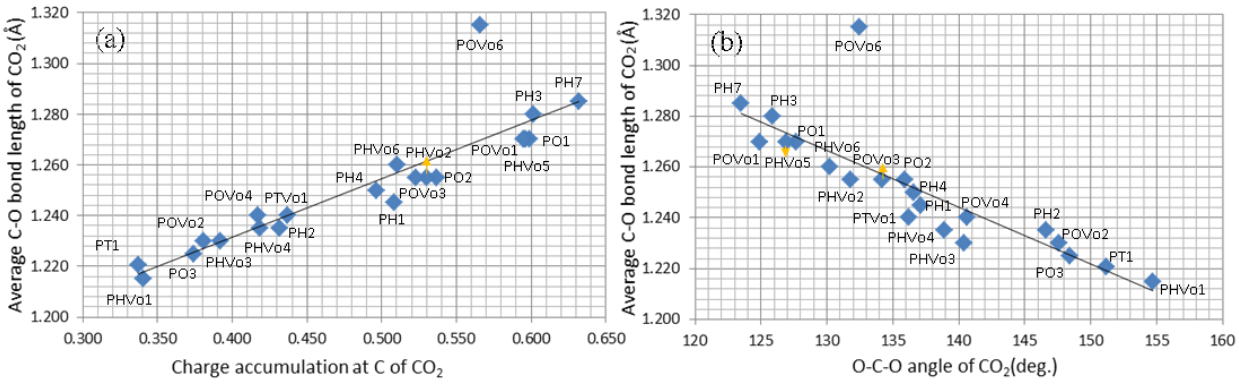

Figure 9. Correlations between the average C-O bond length (bond breaking tendency) and (a) the negative charge accumulation at C, and (b) O-C-O angle of the adsorbed CO_2 species in contact with the supported Pt tetramer, hexamer, and octamer[Octamer data[30]: PO1-PO3(BP1-BP3), POVo1-POVo4(BPVo1-BPVo4), and POVo6(BPVo6); PO, PH, and PT represent Pt octamer, hexamer, and tetramer; Vo represents an oxygen vacancy].

Another correlation of the C-O bond length is found with the angle of O-C-O of CO_2, shown in Figure 9b (the exception to the trend is POVo6, which represents a metastable configuration). The smaller the angle is, the longer the C-O bond. As more electrons accumulate at C of CO_2, these electrons tend to repel the electrons in the C-O bonds, resulting in a smaller O-C-O angle. This is similar to the repulsive character of lone pairs that makes H_2O a bent structure. Note that among 12 interface edge and 9 Pt-only sites, four out of the five longest C-O bonds are interface edge sites, while four out of the five shortest C-O bonds are Pt-only sites. This suggests that the interface sites of the anatase TiO_2 (101) - supported Pt clusters have higher bond-breaking tendency than the Pt-only sites. This correlates with the general tendency of interface edges sites to exhibit stronger bonding (e.g., see Tables 1 and 2).

4.4 Vibrational Frequency

In order to inform experimental spectroscopic studies and provide guidance for photocatalyst design, we have also computed key vibrational frequencies associated with CO_2 adsorption. The vibrational frequencies of symmetric (ν1) and asymmetric (ν3) stretching for adsorbed CO_2 on several metal oxide surfaces have shown relatively good agreement between experimental[69, 70] and computational[28, 30, 33, 36] results; the reported experimental values for the CO_2^- anion were in the ranges of 1219-1247 and 1640-1670 cm^{-1} on P25[70]/anatase TiO_2.[69, 71] We previously revealed that on supported Pt octamer surfaces there are correlations of the ν2 mode with charge accumulation at C of bent-form CO_2, and of the ν3 mode with the O-C-O angle of CO_2.[30] As shown in Figure 10a & b, we confirm that these two correlations still hold true when incorporating adsorbed CO_2 on supported tetramers (PT1 in Figure 1a and PTVo1 in Figure 3a) and hexamers (PH1-PH4 in Figure 2a-d and PHVo1-PHVo2 in Figure 4a&b) alongside the octamer case (PO1-PO3 representing BP1-BP3 in Figure 1d-f, and POVo1-POVo4 representing BPVo1-BPVo4 in Figure 2d-g of our previous work[30]). The sites with the most charge accumulation at C with values around 0.600*e* have ν2 modes in the range of 760-772 cm^{-1}, while smaller charge accumulations around 0.35*e* lie in the 574-602 cm^{-1} range. Likewise, smaller O-C-O angles around 126° lie in the 1483-1529 cm^{-1} range and larger O-C-O angles around 151° in the 1918-1996 cm^{-1} range. We suggest these two trends are general for all supported subnanometer Pt clusters, and that ν2 & ν3 modes can be reliable indicators for electronic and geometric properties of adsorbed CO_2.

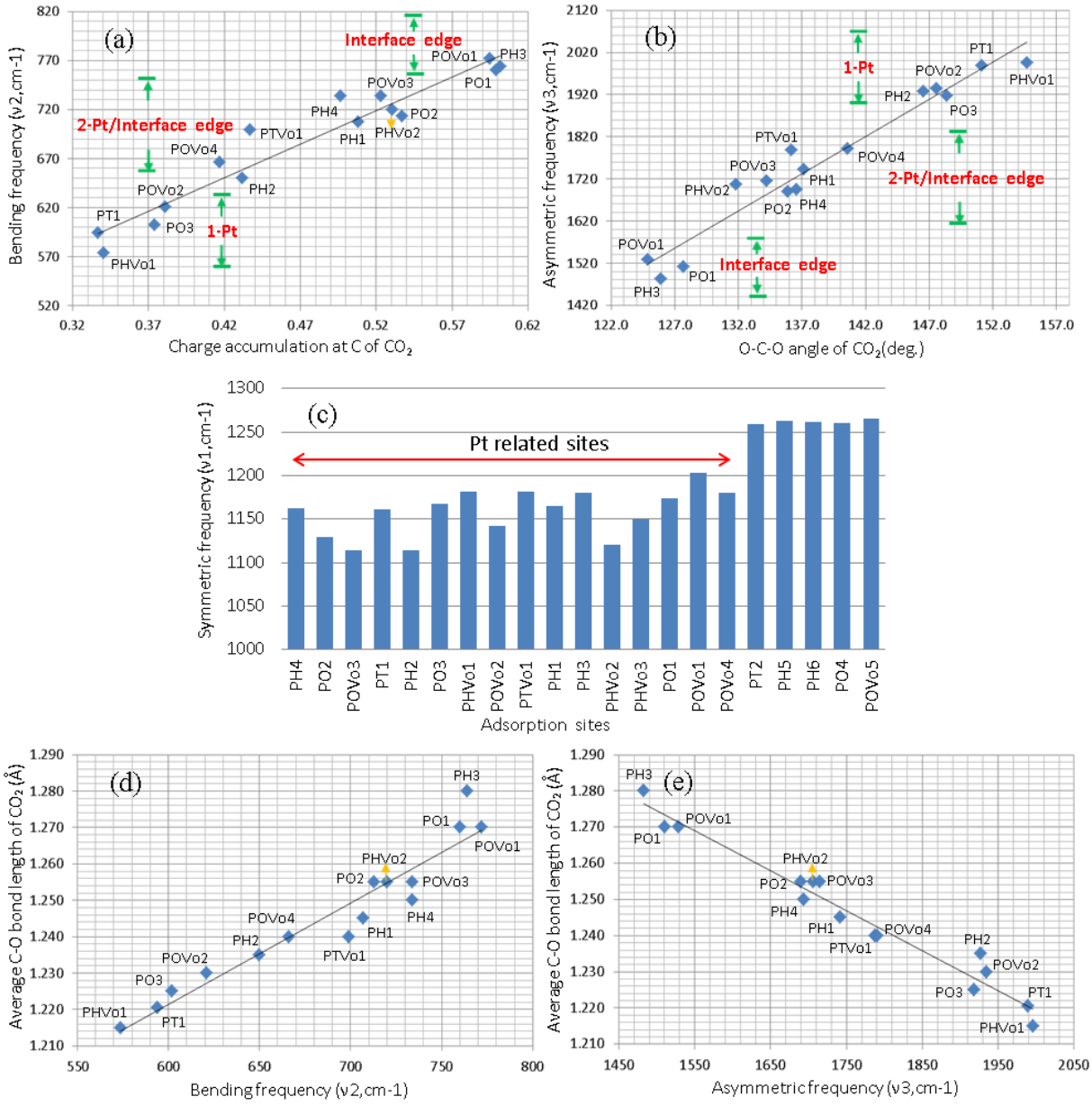

Figure 10. Correlations between (a) the bending frequency (ν2) and the negative charge accumulation at C of CO_2, and between (b) the asymmetric stretching frequency (ν3) and the O-C-O angle of CO_2 for Pt-related binding sites on all tested cluster sizes (tetramer, hexamer, octamer). (c) The symmetric stretching frequency (ν1) for all stable adsorption sites on all cluster sizes, with Pt-related sites highlighted. Correlations between average C-O bond length (indicating bond-breaking tendency) and (d) ν2 and (e) ν3 vibrational frequencies. [Octamer data[30]: PO1-PO4(BP1-BP4) and POVo1-POVo5(BPVo1-BPVo5); PO, PH, and PT represent Pt octamer, hexamer, and tetramer; Vo represents an oxygen vacancy; R2 values for (a), (b), (d), (e) are 0.928, 0.946, 0.918, and 0.9625, respectively].

Here, it is suggested that more detailed information about the nature of the Pt-related adsorption sites (interface edge, 1-Pt only, and 2-Pt only sites) may be found by carefully analyzing the frequencies of the ν2 and ν3 modes. Previously, we showed that ν2 in the range ~750-800 cm^{-1} indicated interface edge adsorption, whereas frequencies below that range indicated Pt octamer-related adsorption; interface edge sites were also revealed by smaller ν3 values (~1500-1540 cm^{-1}).[30] In this study, a similar pattern is observed: ν2 in the lower range (~570-625cm^{-1}) represents 1-Pt only adsorption site; in the higher range (~760-775 cm^{-1}), ν2 signifies interface edge sites, as shown in Figure 10a. However, in between these two ranges, we find that there is a mixed state of interface edge and 2-Pt only sites. An analogous but opposite trend is found for the ν3 mode, as shown in Figure 10b. In this case, ν3 in the higher range (~1910-2000 cm^{-1}) represents 1-Pt only adsorption site; in the lower range (1480-1540 cm^{-1}), ν3 tends to indicate interface edge sites. Likewise, a mixed state of interface edge and 2-Pt only sites also lies in between the ranges. In summary, lower ν2 and higher ν3 reveal 1-Pt only sites, while higher ν2 and lower ν3 reveal interface edge sites, with 2-Pt only sites lying in between the two ranges.

There is some ambiguity following the same analysis of ν2 mode (below ~800 cm^{-1}) for Pt related CO_2 adsorption sites on supported octamers.[30] For instance, as shown in the Supporting Information, though all ν2 modes of the direct TiO_2 surface sites (i.e., not associated with direct Pt contact) are above ~800 cm^{-1}, the threshold for differentiating them from the Pt-associated sites is narrow. Promisingly, the ν1 mode seems to be a more reliable indicator. Shown in Figure 10c are the ν1 frequencies for all stable CO_2 adsorption sites on the supported Pt tetramer, hexamer and octamer, organized according to Pt-related sites (the same sites considered in Figure 10a&b) and direct TiO_2 surface sites (PT2 in Figure 1b, PH5 & PH6 in Figure 2e & f, and

PO4 representing BP4 in Figure 1g and POVo5 representing BPVo5 in Figure 2h of our previous work[30]). As can be clearly seen, ν1 frequencies larger than 1250 cm^{-1} represent direct TiO_2 surface sites, while the collection of Pt-associated sites lies below 1200 cm^{-1}; the lower frequency of the latter may be due to CO_2 stretching inhibited by bonding interactions with Pt clusters, as revealed by DPs in Figure 6.

We have shown the correlations of the C-O bond breaking tendency with negative charge accumulation at C and with O-C-O angle of CO_2 (Figure 9), and that the latter two properties correspond well to specific vibrational frequencies (ν2 and ν3). These data may be combined to develop an experimentally obtainable signal to predict promising CO_2 adsorption sites/configurations with high C-O bond-breaking tendency. Plotted in Figure 10 d & e are the average C-O bond length versus ν2 and ν3 for stable CO_2 adsorption sites on supported tetramers, hexamers, and octamers (the same sites considered in Figure 10a&b). As expected, a strong correlation of the ν2 and ν3 frequencies with C-O bond length can be easily seen, with higher ν2 and lower ν3 suggesting adsorbed CO_2 with longer C-O bonds. These correlations offer valuable information that could be used for experimental understanding of adsorption sites, electronic properties, and catalysis of adsorbed CO_2 species.

5. Conclusions

In summary, the morphology/size (2D or 3D) of Pt tetramers, hexamers, and octamers supported on anatase TiO_2 (101) can significantly affect CO_2 adsorption based on DFT calculations. Compared to flatter 2D Pt clusters, 3D Pt clusters provide more binding sites for bent form CO_2 with electronic charge accumulation at C, which aids in the formation of the key dissociation precursor in CO_2 photoreduction. This geometry-dependent CO_2 adsorption may be explained by considering two key factors: structural fluxionality and binding competition between Pt atoms.

By quantifying structural fluxionality based on the adsorbate-induced displacement, we find that at interface edge sites, 3D clusters tend to have higher structural fluxionality than 2D-like clusters. This is because the top layer atoms of the 3D cluster are less constrained compared to the 2D cluster. High fluxionality capability is also related to stronger CO_2 binding, since geometric reconstruction enables maximum orbital overlap between the Pt clusters and CO_2. Binding competition can occur when more than one Pt atom attempt to bind with CO_2. If structural fluxionality is inhibited, as is the case for binding on 2D-like surfaces, then competition between the Pt atoms may mitigate maximum orbital overlap among each individual Pt-CO_2 bonding interaction, leading to instability.

Interestingly, we also find that there is a dependence of the cluster geometry and morphology on the nature of the host surface. In particular, when Pt tetramers and hexamers deposit on perfect anatase TiO_2 (101), they exhibit a 3D structure, whereas on the reduced surface, a 2D-like structure is favored. This is due to Pt cluster's strong disposition to bind with more surface Ti atoms, which are exposed by the presence of surface oxygen vacancies. The differences between the morphologies of the clusters on perfect and reduced surfaces lead to qualitatively different behaviors in CO_2 binding.

Electronic structure analysis indicates that the main bonding states for CO_2 on TiO_2-supported subnanometer Pt clusters come from CO_2 s&p - metal d state interactions. However, we also find that CO_2 binding strength has little to do with the number of Pt atoms involved. Interface edge sites have stronger CO_2 binding than Pt-only sites, and such enhancement may be due to extra bonding interaction with the surface oxygen atom. Furthermore, to make CO_2 activation feasibly lead to the desired products of CO_2 photoreduction, C-O bond breaking is critical, which results from the filling of antibonding orbitals of the CO_2 molecule.[30] We

demonstrate that this bond-breaking tendency is related to charge accumulation at C and the O-C-O angle of the adsorbed CO_2 species, which in turn are dependent on the interplay between the cluster geometry and available binding sites. These factors are detectable in key signatures in the ν1, ν2, and ν3 vibrational frequencies (previously reported for octamers[30] and confirmed here to be a more general rule), from which specific binding sites and geometries may be identified experimentally. Our results may be used towards practical design of promising CO_2 reduction photocatalysts in subnanometer metal/semiconductor frameworks.

Acknowledgements

The authors also wish to thank the USF supercomputing center for computing time and support. A portion of this work was performed under the auspices of the U.S. Department of Energy by Lawrence Livermore National Laboratory under Contract DE-AC52-07NA27344.

References

1. H. Hakkinen, W. Abbet, A. Sanchez, U. Heiz and U. Landman, *Angew. Chem. Int. Ed.* 2003, **42**, 1297- 1300.
2. B. Yoon, H. Hakkinen, U. Landman, A. S. Worz, J. M. Antonietti, S. Abbet, K. Judai and U. Heiz, *Science*, 2005, **307**, 403-407.
3. S. Vajda, M. J. Pellin, J. P. Greeley, C. L. Marshall, L. A. Curtiss, G. A. Ballentine, J. W. Elam, S. Catillon-Mucherie, P. C. Redfern, F. Mehmood and P. Zapol, *Nat. Mater.*, 2009, **8**, 213-216.
4. B. T. Qiao, A. Q. Wang, X. F. Yang, L. F. Allard, Z. Jiang, Y. T. Cui, J. Y. Liu, J. Li and T. Zhang, *Nat. Chem.*, 2011, **3**, 634-641.
5. Y. Lei, F. Mehmood, S. Lee, J. Greeley, B. Lee, S. Seifert, R. E. Winans, J. W. Elam, R. J. Meyer, P. C. Redfern, D. Teschner, R. Schlogl, M. J. Pellin, L. A. Curtiss and S. Vajda, *Science*, 2010, **328**, 224-228.
6. T. Imaoka, H. Kitazawa, W. J. Chun, S. Omura, K. Albrecht and K. Yamamoto, *J. Am. Chem. Soc.*, 2013, **135**, 13089-13095.
7. S. J. Tauster, *Acc. Chem. Res.*, 1987, **20**, 389-394.
8. G. A. Ferguson, F. Mehmood, R. B. Rankin, J. P. Greeley, S. Vajda and L. A. Curtiss, *Top. Catal.* 2012, **55**, 353-365.
9. C. T. Yang, N. Balakrishnan, V. R. Bhethanabotla and B. Joseph, *J. Phys. Chem. C*, 2014, **118**, 4702- 4714.

10. X. Q. Gong, A. Selloni, O. Dulub, P. Jacobson and U. Diebold, *J. Am. Chem. Soc.*, 2008, **130**, 370-381.
11. S. C. Ammal and A. Heyden, *J. Chem. Phys.*, 2010, **133**, 164703.
12. J. Zhang and A. N. Alexandrova, *J. Chem. Phys.*, 2011, **135**, 174702.
13. A. Fujishima and K. Honda, *Nature*, 1972, **238**, 37-38.
14. I. K. Konstantinou and T. A. Albanis, *Appl. Catal., B*, 2004, **49**, 1-14.
15. B. Aurianblajeni, M. Halmann and J. Manassen, *Sol. Energy*, 1980, **25**, 165-170.
16. Z. Zou, J. Ye, K. Sayama and H. Arakawa, *Nature*, 2001, **414**, 625-627.
17. M. A. Henderson, *Surf. Sci. Rep.*, 2011, **66**, 185-297.
18. Z. Yi, J. Ye, N. Kikugawa, T. Kako, S. Ouyang, H. Stuart-Williams, H. Yang, J. Cao, W. Luo, Z. Li, Y. Liu and R. L. Withers, *Nat. Mater.*, 2010, **9**, 559-564.
19. S. Ouyang and J. Ye, *J. Am. Chem. Soc.*, 2011, **133**, 7757-7763.
20. P. Niu, L. Zhang, G. Liu and H.-M. Cheng, *Adv. Funct. Mater.*, 2012, **22**, 4763-4770.
21. A. Sclafani and J.-M. Herrmann, *J. Photochem. Photobiol., A*, 1998, **113**, 181-188.
22. Linic, P. Christopher and D. B. Ingram, *Nat. Mater.*, 2011, **10**, 911-921.
23. W. Hou, W. H. Hung, P. Pavaskar, A. Goeppert, M. Aykol and S. B. Cronin, *ACS Catal.*, 2011, **1**, 929-936.
24. A. L. Linsebigler, G. Lu and J. T. Yates, *Chem. Rev.*, 1995, **95**, 735-758.
25. X. Zhang, J. Qin, Y. Xue, P. Yu, B. Zhang, L. Wang and R. Liu, *Sci. Rep.*, 2014, **4**, 4596.
26. A. Markovits, A. Fahmi and C. Minot, *J. Mol. Struct. THEOCHEM*, 1996, **371**, 219-235.
27. V. P. Indrakanti, J. D. Kubicki and H. H. Schobert, *Energy Environ. Sci.*, 2009, **2**, 745-758.
28. H. He, P. Zapol and L. A. Curtiss, *J. Phys. Chem. C*, 2010, **114**, 21474-21481.
29. D. Lee and Y. Kanai, *J. Am. Chem. Soc*, 2012, **134**, 20266-20269.
30. C. T. Yang, B. C. Wood, V. Bhethanabotla and B. Joseph, *J. Phys. Chem. C*, 2014, **118**, 26236–26248.
31. P. Usubharatana, D. McMartin, A. Veawab and P. Tontiwachwuthikul, *Ind. Eng. Chem. Res.*, 2006, **45**, 2558-2568.
32. V. P. Indrakanti, J. D. Kubicki and H. H. Schobert, *Energy Fuels*, 2008, **22**, 2611-2618.
33. M. M. Rodriguez, X. H. Peng, L. J. Liu, Y. Li and J. M. Andino, *J. Phys. Chem. C*, 2012, **116**, 19755-19764.
34. W. Pipornpong, R. Wanbayor and V. Ruangpornvisuti, *Appl. Surf. Sci.*, 2011, **257**, 10322-10328.
35. L. Mino, G. Spoto and A. M. Ferrari, *J. Phys. Chem. C*, 2014, **118**, 25016-25026.
36. Dan C. Sorescu, W. A. A.-S., and Kenneth D. Jordan, *J. Chem. Phys.*, 2011, **135**, 124701.
37. L. Liu, W. L. Fan, X. Zhao, H. G. Sun, P. Li and L. M. Sun, *Langmuir*, 2012, **28**, 10415-10424.
38. Z. Cheng, B. J. Sherman and C. S. Lo, *J. Chem. Phys.*, 2013, **138**, 014702.
39. K. R. Hahn, M. Iannuzzi, A. P. Seitsonen and J. Hutter, *J. Phys. Chem. C*, 2013, **117**, 1701-1711.
40. X. Tong, L. Benz, P. Kemper, H. Metiu, M. T. Bowers and S. K. Buratto, *J. Am. Chem. Soc.*, 2005, **127**, 13516-13518.
41. M. Valden, X. Lai and D. W. Goodman, *Science*, 1998, **281**, 1647-1650.
42. Y. Watanabe, X. Y. Wu, H. Hirata and N. Isomura, *Catal. Sci. Technol.*, 2011, **1**, 1490-1495.
43. U. Heiz, A. Sanchez, S. Abbet and W. D. Schneider, *J. Am. Chem. Soc.*, 1999, **121**, 3214-3217.
44. S. S. Lee, C. Y. Fan, T. P. Wu and S. L. Anderson, *J. Am. Chem. Soc.*, 2004, **126**, 5682-5683.

45. W. E. Kaden, T. P. Wu, W. A. Kunkel and S. L. Anderson, *Science*, 2009, **326**, 826-829.
46. A. A. Herzing, C. J. Kiely, A. F. Carley, P. Landon and G. J. Hutchings, *Science*, 2008, 321, 1331-1335.
47. A. Selloni, *Nat. Mater.*, 2008, **7**, 613-615.
48. G. Kresse and J. Furthmuller, *Comp. Mater. Sci.*, 1996, **6**, 15-50.
49. G. Kresse and J. Furthmuller, *Phys. Rev. B*, 1996, **54**, 11169-11186.
50. G. Kresse and J. Hafner, *Phys. Rev. B*, 1993, **47**, 558-561.
51. J. P. Perdew, K. Burke and M. Ernzerhof, *Phys. Rev. Lett.*, 1996, **77**, 3865-3868.
52. P. E. Blochl, *Phys. Rev. B*, 1994, **50**, 17953-17979.
53. V. I. Anisimov and O. Gunnarsson, *Phys. Rev. B*, 1991, **43**, 7570-7574.
54. D. Cakir and O. Gulseren, *J. Phys. Chem. C*, 2012, **116**, 5735-5746.
55. Y. Han, M. Zhang, W. Li and J. L. Zhang, *Phys. Chem. Chem. Phys.*, 2012, **14**, 8683-8692.
56. U. Aschauer, Y. B. He, H. Z. Cheng, S. C. Li, U. Diebold and A. Selloni, *J. Phys. Chem. C*, 2010, **114**, 1278-1284.
57. H. J. Monkhorst and J. D. Pack, *Phys. Rev. B*, 1976, **13**, 5188-5192.
58. E. Sanville, S. D. Kenny, R. Smith and G. Henkelman, *J. Comput. Chem.*, 2007, **28**, 899-908.
59. R. Wanbayor, P. Deak, T. Frauenheim and V. Ruangpornvisuti, *J. Chem. Phys.*, 2011, **134**, 104701.
60. D.-e. Jiang, S. H. Overbury and S. Dai, *J. Phys. Chem. C*, 2012, **116**, 21880-21885.
61. B. Hammer and J. K. Norskov, *Nature*, 1995, **376**, 238-240.
62. A. Nilsson, L. G. M. Pettersson, B. Hammer, T. Bligaard, C. H. Christensen and J. K. Norskov, *Catal. Lett.*, 2005, **100**, 111-114.
63. H. J. Freund and M. W. Roberts, *Surf. Sci. Rep.*, 1996, **25**, 225-273.
64. G. Illing, D. Heskett, E. W. Plummer, H. J. Freund, J. Somers, T. Lindner, A. M. Bradshaw, U. Buskotte, M. Neumann, U. Starke, K. Heinz, P. L. Deandres, D. Saldin and J. B. Pendry, *Surf. Sci.*, 1988, **206**, 1-19.
65. X. Lin, Y. Yoon, N. G. Petrik, Z. J. Li, Z. T. Wang, V. A. Glezakou, B. D. Kay, I. Lyubinetsky, G. A. Kimmel, R. Rousseau and Z. Dohnalek, *J. Phys. Chem. C*, 2012, **116**, 26322-26334.
66. M. Buchholz, P. G. Weidler, F. Bebensee, A. Nefedov and C. Woll, *Phys. Chem. Chem. Phys.*, 2014, **16**, 1672-1678.
67. M. J. T. Frisch, G. W.; Schlegel, H. B.; Scuseria, G. E.; Robb, M. A.; Cheeseman, J. R.; Scalmani, G.; Barone, V.; Mennucci, B.; Petersson, G. A.; Nakatsuji, H.; Caricato, M.; Li, X.; Hratchian, H. P.; Izmaylov, A. F.; Bloino, J.; Zheng, G.; Sonnenberg, J. L.; Hada, M.; Ehara, M.; Toyota, K.; Fukuda, R.; Hasegawa, J.; Ishida, M.; Nakajima, T.; Honda, Y.; Kitao, O.; Nakai, H.; Vreven, T.; Montgomery, Jr., J. A.; Peralta, J. E.; Ogliaro, F.; Bearpark, M.; Heyd, J. J.; Brothers, E.; Kudin, K. N.; Staroverov, V. N.; Kobayashi, R.; Normand, J.; Raghavachari, K.; Rendell, A.; Burant, J. C.; Iyengar, S. S.; Tomasi, J.; Cossi, M.; Rega, N.; Millam, J. M.; Klene, M.; Knox, J. E.; Cross, J. B.; Bakken, V.; Adamo, C.; Jaramillo, J.; Gomperts, R.; Stratmann, R. E.; Yazyev, O.; Austin, A. J.; Cammi, R.; Pomelli, C.; Ochterski, J. W.; Martin, R. L.; Morokuma, K.; Zakrzewski, V. G.; Voth, G. A.; Salvador, P.; Dannenberg, J. J.; Dapprich, S.; Daniels, A. D.; Farkas, Ö.; Foresman, J. B.; Ortiz, J. V.; Cioslowski, J.; Fox, D. J., *Gaussian 09; Gaussian, Inc.,Wallingford CT*, 2009.
68. A. E. Reed, L. A. Curtiss and F. Weinhold, *Chem. Rev.*, 1988, **88**, 899-926.
69. W. G. Su, J. Zhang, Z. C. Feng, T. Chen, P. L. Ying and C. Li, *J. Phys. Chem. C*, 2008, **112**, 7710-7716.

70. J. Rasko and F. Solymosi, *J. Chem. Phys.*, 1994, **98**, 7147-7152.
71. L. J. Liu, H. L. Zhao, J. M. Andino and Y. Li, *ACS Catal.*, 2012, **2**, 1817-1828.